

# Multiple Coulomb phases with temperature tunable ice rules in pyrochlore spin crossover materials

Jace Cruddas\* and B. J. Powell†

*School of Mathematics and Physics, The University of Queensland, QLD 4072, Australia*

Spin crossover molecules have two accessible states: high spin (HS) and low spin (LS). We show that, on the pyrochlore lattice, elastic interactions between SCO molecules can give rise to three spin-state ice phases. Each is a ‘‘Coulomb phase’’ where a local ice-rule can be mapped to a divergence free gauge field and the low energy excitations carry a spin fractionalized midway between the LS and HS states. The unique nature of spin crossover materials allows temperature to change the ice rules allowing straightforward access to Coulomb phases not yet observed in water or spin ices.

In spin ices, such as  $\text{Dy}_2\text{Ti}_2\text{O}_7$  and  $\text{Ho}_2\text{Ti}_2\text{O}_7$ , the magnetic Dy (Ho) atoms form a pyrochlore lattice composed of vertex sharing tetrahedra. The combination of the crystal field and the long-range dipolar interaction constrain the magnetic moments to obey the 2-in/2-out ice rule: Two of the spins point into each tetrahedron and two point out. The ice rule can be mapped onto a divergence-free flux, analogous to constraints in magnetostatics and electrostatics. Violations of the ice rule carry a fraction of the magnetic spin degree of freedom, behaving effectively as magnetic monopoles with an emergent Coulombic interaction between them [1]. Spin ices are therefore said to be in a ‘‘Coulomb phase’’, which could also arise in frustrated antiferromagnets and some quantum spin liquids [2, 3].

In principle ices obeying 1-in/3-out or 3-in/1-out ice rules should also give rise to Coulomb phases. This has not yet been observed, although an ordered phase containing 1-in/3-out and 3-in/1-out tetrahedra has been reported [4]. For the nearest neighbor Ising model on the pyrochlore lattice with collinear spins,  $S_i$ , then, up to a constant,

$$\mathcal{H}_I = J \sum_{\langle i,j \rangle} S_i S_j + B \sum_i S_i = J \sum_{\alpha} (L_{\alpha} + B/4J)^2, \quad (1)$$

where  $L_{\alpha} = \sum_{i \in \alpha} S_i$  and  $\alpha$  labels the tetrahedra. The ground state is clearly achieved whenever the magnitude of the ‘flux’,  $L_{\alpha} + B/4J$ , is minimized for all  $\alpha$ . Ice rules require the same value of  $L_{\alpha}$  on all tetrahedra. Therefore, sweeping  $B$  moves the ground state between different ice rules. However, in spin ices the spins are not collinear and so one cannot simply apply a magnetic field to change the ice-rules in these systems.

Recently, it has been proposed that spin-state ices can occur in spin-crossover materials [5]. In this Letter we show that multiple Coulomb phases arise for spin-crossover materials on the pyrochlore lattice. Furthermore, we show that sweeping *temperature* alone is sufficient to tune between Coulomb phases obeying three different ice rules. This is a direct consequence of the competition between the single molecule spin crossover behavior and the many-body ice physics. We predict that pinch point singularities, the *sine qua non* of the Coulomb phase, will be

detectable via neutron scattering in small magnetic fields and that the low-energy excitations are deconfined and carry a spin midway between the that of the two spin states of a single molecule.

Spin crossover (SCO) occurs in transition metal centers in complexes and frameworks when the low-spin (LS; e.g.,  $t_{2g}^6 e_g^0$ ,  $S = 0$ ) and high-spin (HS; e.g.,  $t_{2g}^4 e_g^2$ ,  $S = 2$ ) states have comparable enthalpy. SCO provides a reversible molecular switch, which is addressable by changes in temperature, pressure, light irradiation, magnetic field, and chemical environment [6]. As spin-state changes are accompanied by changes in molecular volume, color, and magnetic susceptibility, SCO materials are intrinsically multifunctional and have been widely explored for applications such as high-density reversible memory, and ultrafast nanoscale switches [6–8]. However, many questions about the fundamental physics at play in these systems remain open [9–23].

Changes in the molecular volume accompany spin-state switching due to the (de)population of antibonding  $e_g$  orbitals in the (LS) HS state: the metal-ligand bond length in the HS state is often  $\sim 10\%$  larger than that in the LS state. In molecular materials and frameworks, the local structural distortions caused by metals changing spin state couple to long-range elastic interactions. It is convenient to introduce a pseudospin label for the spin state of each metal,  $\sigma_i = 1$  ( $-1$ ) if the  $i$ th molecule is HS (LS). Because  $\sigma_i^2 = 1$  no terms above quadratic order appear in pairwise interactions [23]. Letting  $R_H$  ( $R_L$ ) be the equilibrium distance between metals in the HS (LS) phases, we can write the equilibrium midpoint between neighboring metals as  $\bar{R} + \delta(\sigma_i + \sigma_j)$ , where,  $\bar{R} = (R_H + R_L)/2$  and  $\delta = (R_H - R_L)/2$ . Hence,

$$\mathcal{H} = \frac{\Delta H}{2} \sum_i \sigma_i + \sum_{n=1}^m \frac{k_n}{2} \sum_{\langle i,j \rangle_n} \{r_{ij} - \eta_n [\bar{R} + \delta(\sigma_i + \sigma_j)]\}^2, \quad (2)$$

where  $\Delta H = H_H - H_L$  is the enthalpy difference between HS and LS metals and  $k_n$  are the effective spring constants between  $n$ th nearest neighbors (see Fig. 1), the sum over  $\langle i,j \rangle_n$  includes all  $n$ th nearest-neighbors,  $r_{ij}$  is the instantaneous distance between sites  $i$  and  $j$ , and  $\eta_n = 1, \sqrt{3}, 2, \dots$  is the ratio of distances between

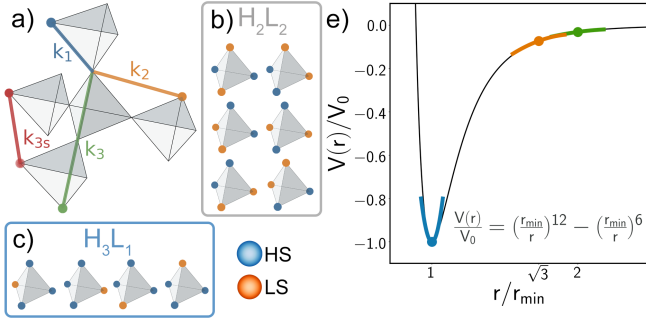


FIG. 1. (a) Pyrochlore lattice with the three nearest neighbor interactions ( $k_1$ ,  $k_2$ , and  $k_3$ ) marked. We neglect through-space interactions between third nearest neighbors,  $k_{3s}$ , as we expect these to be much weaker than  $k_3$ . Ice rules in the (b)  $H_2L_2$  and (c)  $H_1L_3$  phases. (d) Near the minimum of the potential between neighboring metals  $\partial^2 V(r)/\partial r^2 \simeq k_1$ , is positive and large. At larger distances the second derivative is negative and decreases in magnitude with increasing distances. Therefore, one expects  $k_1 > 0$  and  $k_2 < k_3 < 0$  for the pyrochlore lattice. At larger distances the higher order (non-harmonic) contributions to the potential simply re-normalize  $\Delta H$  and  $k_n$  because  $\sigma_i^2 = 1$ .

the  $n$ th and 1st nearest-neighbor distances on the undistorted pyrochlore lattice. Inspired by recent progress in the synthesis of tetrahedral iron cages [24] we study this model with  $m = 3$  on the pyrochlore lattice (Fig. 1a), where we expect  $k_2 < k_3 < 0$  (Fig. 1d) and require  $k_1 + 6k_2 + 4k_3 > 0$  for structural stability.

There are two contributions to the entropy. The usual many-body entropy described by the configuration of the  $\sigma_i$  and a single molecule term,  $\Delta S$ , due to changes in the spin and orbital quantum numbers and vibrational frequencies between the HS and LS states. Below we set  $\Delta S = 4 \ln 5$ , a typical value of Fe(II) complexes [25]. It is convenient to define  $\Delta G = \Delta H - T\Delta S$  and absorb this term into the Hamiltonian [26]. We make the ‘symmetric breathing mode approximation’, which neglects asymmetric structural distortions [5, 23], and calculate the finite temperature properties from a combination of single spin-flip Monte Carlo, worm and loop algorithms and parallel tempering on a  $12 \times 12 \times 12 \times 4$  lattice except where stated.

The weak magnetic interactions in most SCO materials means that the fraction of HS molecules,  $n_{HS} \sim \chi T$ . Hence the magnetic susceptibility,  $\chi$ , is commonly used as a diagnostic for the cooperative behavior in the system. Strong cooperative behaviors often give rise to multiple step transitions [6, 27–30]. Typically, when  $k\delta^2 \sim k_B T_{1/2}$  [23], where  $T_{1/2} = \Delta H/\Delta S$ , the temperature at which one expects  $n_{HS} = 1/2$ , is typically 100-400 K. The intermediate plateaus often display long-range patterns of HS and LS metals. But, several disordered phases have been reported also [31–33].

We find three distinct spin-state ice (SSI) phases:

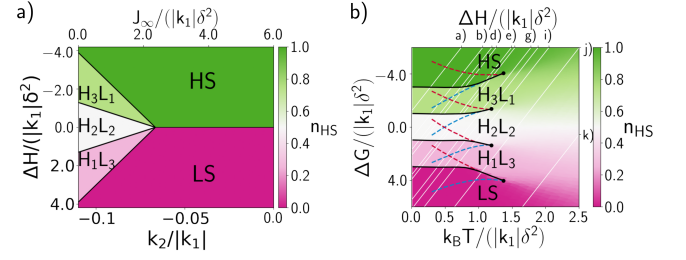


FIG. 2. a) The zero phase diagram for  $k_1 > 0$  and  $k_3 = 3k_2/4$ . For small  $|k_2|$  the long-range strain dominates and picks out a ferroelastic state, but large  $|k_2|$  suppresses this effect allowing the spin-state ices to emerge. b) The finite temperature phase diagram for  $k_1 > 0$ ,  $k_2 = -0.1k_1$ , and  $k_3 = 0.075k_1$ . The colors of the phase diagram indicate the equilibrium values of the fraction of high spins  $n_{HS}$ , calculated via parallel tempering. We find four (black) lines of first order transitions that terminate at critical end points (black circles). The blue and red lines indicate lines of metastability for the cooling and heating calculations, respectively, cf. Fig. S3 [34]. Hence, the distance between blue and red lines is the width of the hysteresis. Individual materials have a fixed  $\Delta H$  (white lines), the corresponding HS fractions,  $n_{HS}$ , and heat capacities are shown in Fig. 4 and Fig. S2 [34], respectively.

$H_3L_1$ ,  $H_2L_2$  and  $H_1L_3$ , see Fig. 2 [34]. In the ground state of the  $H_nL_{4-n}$  phase every tetrahedron contains  $n$  HS and  $4-n$  LS metals (Fig. 1b-c). Thus, the  $H_3L_1$  and  $H_1L_3$  phases can be mapped onto the dimer model on a diamond lattice, and the  $H_2L_2$  phase can be mapped onto the loop model on a diamond lattice [2].

In order to verify the phases at  $T = 0$  are indeed Coulomb phases we have calculated the pseudo-spin structure factor, Fig. 3j-l,

$$S_{\sigma\sigma}(\vec{q}) = \frac{1}{N} \sum_{ij} \langle \sigma_i \sigma_j \rangle e^{i\vec{q} \cdot \vec{r}_{ij}}. \quad (3)$$

We clearly observe singularities in  $S_{\sigma\sigma}$  at the Brillouin zone boundary, known as pinch points, which are a direct consequence of the existence of a divergenceless gauge field [2]. This confirms that the intermediate plateaus are indeed Coulomb phases.

However, directly measuring the pseudospin structure factor is not straightforward. In SCO materials the magnetic correlations between sites are typically negligible. Therefore, the spins are described by a Zeeman Hamiltonian,  $\mathcal{H}_Z = \sum_i \mu_B^z B \mathbf{S}_i^z(\sigma_i)$ , where the spin,  $\mathbf{S}_i(\sigma_i)$ , depends on the spin-state,  $B$  is the applied field, and  $\mu_B$  is Bohr magneton. The spin structure factor is

$$S_{SS}(\vec{q}) \equiv \frac{1}{N} \sum_{ij} \langle \mathbf{S}_i(\sigma_i) \cdot \mathbf{S}_j(\sigma_j) \rangle e^{i\vec{q} \cdot \vec{r}_{ij}} \quad (4a)$$

$$= [m_+^2 + m_-^2 - 2m_+m_-] \frac{S_{\sigma\sigma}(\vec{q})}{4} + S_d(B^z) + S_B(B^z)\delta(q), \quad (4b)$$

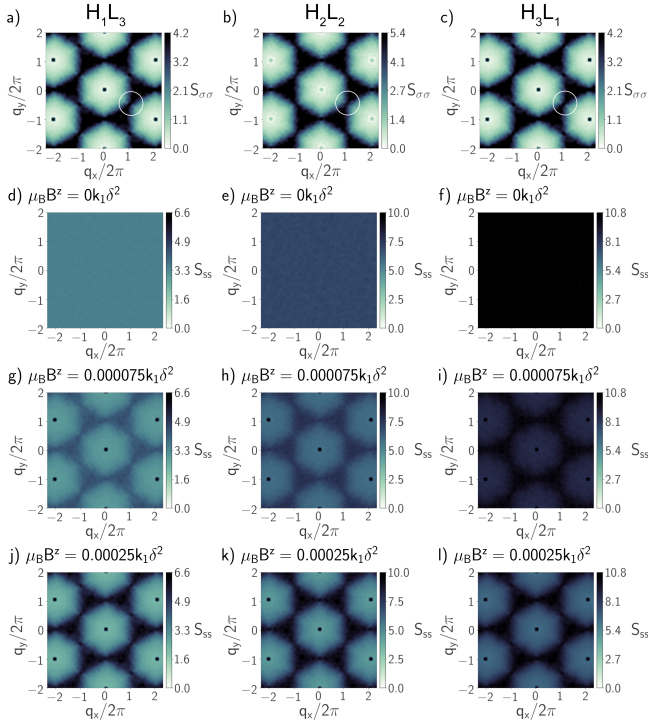


FIG. 3. (a-c) The pseudospin structure factors,  $S_{\sigma\sigma}$ , Eq. 3, for (a)  $H_1L_3$ , (b)  $H_2L_2$ , and (c)  $H_3L_1$ . All structure factors display pinch points, one of which is circled, at the Brillouin zone boundaries characteristic of a Coulomb phase. The existence of the pinch points demonstrates that the low-energy physics of Coulomb phases are described by a divergence-less gauge field [2]. (d-l) The spin structure factors,  $S_{SS}$ , Eq. 4, for (d,g,j)  $H_1L_3$ , (e,h,k)  $H_2L_2$ , and (f,i,l)  $H_3L_1$  at selected magnetic field strengths. For  $k\delta^2 \sim 100$  K the calculations are  $< 0.1$  T, so only moderate fields are required for the pinch points to be observable via neutron scattering. All structure factors were calculated for  $k_1 > 0$ ,  $k_2/k_1 = 4k_3/3k_1 = -0.1$  and  $k_B T/(k_1\delta^2) = 0.01$  on a  $36 \times 36 \times 4 \times 4$  lattice with (a,d,g,j)  $\Delta H = 2k_1\delta^2$ , (b,e,h,k)  $\Delta H = 0$  and (c,f,i,l)  $\Delta H = -2k_1\delta^2$ .

where  $m_{\pm} = \sum_i \langle S_i^z(\pm 1) \rangle / N$ , and expressions for the trivial diffuse,  $S_d(B^z)$  and Bragg,  $S_B(B^z)$ , scattering are given in [34]. This, is directly measurable via neutron scattering and clearly shows the pinch points, Fig. 3. We note that the fields required are modest. For  $k\delta^2 \sim 100$  K the calculations are  $< 0.1$  T.

The ratio  $\Delta H/(\delta^2 k_1)$  not only has important consequences for the low-temperature physics, but also for the high-temperature behavior as well, Figs. 2b and 4. For  $\Delta H \sim -(k_1\delta^2)$  we observe a single first order transition. This is a purely collective phenomena, as the single ion physics always favors the HS state ( $\Delta G < 0 \forall T$ ). Increasing  $\Delta H$  induces further transitions with plateaus at  $n_{HS} \simeq 0, \frac{1}{4}, \frac{1}{2}, \frac{3}{4}$  and 1, corresponding to the LS,  $H_1L_3$ ,  $H_2L_2$ ,  $H_3L_1$  and HS phases respectively, 4b-h. Hence, for a wide range of parameters, it is possible to tune between different Coulomb phases with temperature alone.

This can be understood as follows: The single molecule

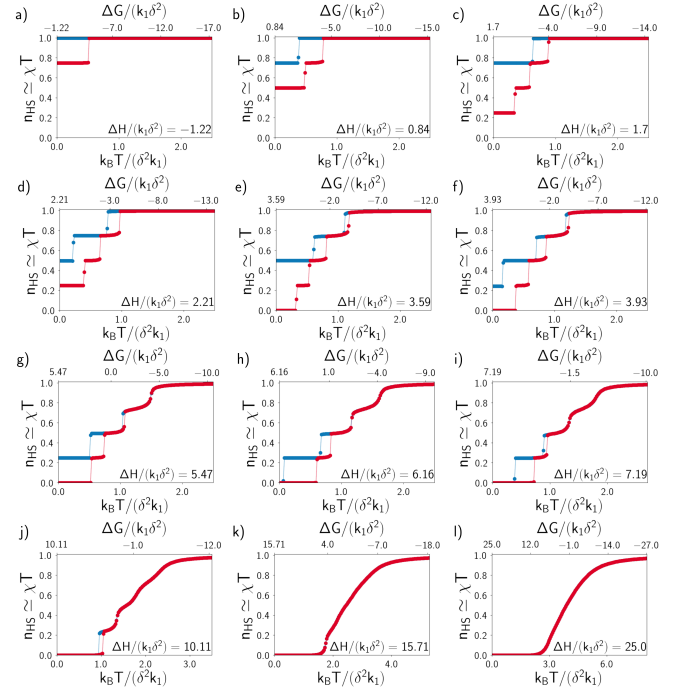


FIG. 4. The fraction of high spins,  $n_{HS}$ , for selected values of  $\Delta H/(k_1\delta^2)$  with  $k_1 > 0$  and  $k_2/k_1 = 4k_3/3k_1 = -0.1$ . The red and blue lines represent heating and cooling respectively. We find plateaus at  $n_{HS} \simeq 0, \frac{1}{4}, \frac{1}{2}, \frac{3}{4}$  and 1, corresponding to the LS,  $H_1L_3$ ,  $H_2L_2$ ,  $H_3L_1$ , and HS phases. Hence, for a wide range of parameters, it is possible to tune between different Coulomb phases with temperature alone.

entropy difference between spin-states ( $\Delta S$ ) can be absorbed into the Hamiltonian [26]. Thus,  $\Delta G = \Delta H - T\Delta S$  replaces  $\Delta H$  in Eq. (2). This term couples to the pseudospin just as a magnetic field couples to spin in the Ising model, Eq. (1). That is, the single molecule spin crossover behavior acts as an effective temperature-dependent ‘field’ for the pseudospins. This changes the ice rules as the temperature varies.

Due to the large width of the hysteresis loop at low temperatures, simulations of straightforward cooling does not always result in the same low temperature phase as is found by parallel tempering, Fig. 4a-g. Similar effects have been observed experimentally in SCO materials that display long-range antiferroelastic order [35], and labeled “hidden hysteresis”. The hidden low temperature states can be realized by either photoswitching (i.e., reverse-light induced excited spin-state trapping) or applying and adiabatically releasing a pressure to the system. Hence, it becomes possible to tune between different SSI phases with not only temperature but, pressure and light as well.

Further increasing  $\Delta H/(k_1\delta^2)$  moves the transitions towards and through critical points, where the transition is continuous, and into the crossover regime, Figs. 2b and 4g-i. The higher temperature transitions be-

come crossovers first as  $\Delta H/(k_1\delta^2)$  increases until there is eventual only a single crossover. This results in significant melting of the SSI phases and the spontaneous production of defects. For each SSI phase there are two different types of defects. For a state obeying the spin-state ice rules everywhere changing a metal from a LS to HS state creates a  $h$ -defect on both of the tetrahedra connected to the metal center, Fig. 5a,b. Conversely, changing the spin-state of a metal from HS to LS creates two  $l$ -defects.

To understand these defects it is helpful to consider a large magnetic field in the  $z$  direction, such that  $S_i^z(1) = S_H$  and  $S_i^z(-1) = S_L$ . The creation of two  $h$  defects increase the number of HS metals by one. Thus, each defect carries a spin  $\frac{1}{2}(S_H - S_L) \equiv \delta S$ . Similarly, the process of creating two  $l$  defects on the connected tetrahedra corresponds to the creation of two quasi-particles with spin  $-\delta S$ . It is important to note that there are no intermediate spin-states in the model. Hence, these defects arise purely as a collective effect and thus correspond to fractionalized quasi-particles with spin midway between HS and LS states.

The multiple of ways to satisfy the spin-state ice rules allow defects to propagate, Fig. 5. For example, a metal center changing from HS to LS on a tetrahedron containing a  $h$  defect restores the ice rules on that tetrahedron and creates a  $l$  defect on the other tetrahedron connected to the metal center, Fig. 5b,c. Thus, the number of  $h$  and  $l$  type defects are not conserved. However, the topological charge  $Q = \kappa\delta S$  is conserved, where  $\kappa = \pm 1$  for tetrahedra pointing in the  $\pm z$  direction. It only takes a finite amount of energy to move a pair of defects infinitely far apart. Hence, the fractionalized topological charges are deconfined [2].

$h$  and  $l$  defects carry the opposite spin. Therefore, if  $\delta S$  and  $-\delta S$  topological charges meet on the same tetrahedron they annihilate, restoring the spin-state ice rules.

It has recently been show that strain can induce the motion of domain walls in ordered phases of SCO materials [36]. This is likely a consequence of the volume difference in the HS and LS states. Suggesting that strain should also induce motion of the defects in SSI Coulomb phases. Alternatively, spin-orbit coupling should couple the quasiparticles to an applied voltage. Either of these effects could make SSI a valuable resource for spintronic applications.

Our calculations predict that three distinct Coulomb phases arise in pryochnore lattices in extended regions of both the zero-temperature and finite temperature phase diagrams. In each phase the low energy excitations are mobile and deconfined, carrying a spin midway between that of the HS and LS states. Realizing Coulomb phases beyond the 2-in/2-out phases in water and spin ices has proven extremely challenging. However, the unique role of the single molecule entropy in spin crossover materials allows temperature to change the ice rules. The physics

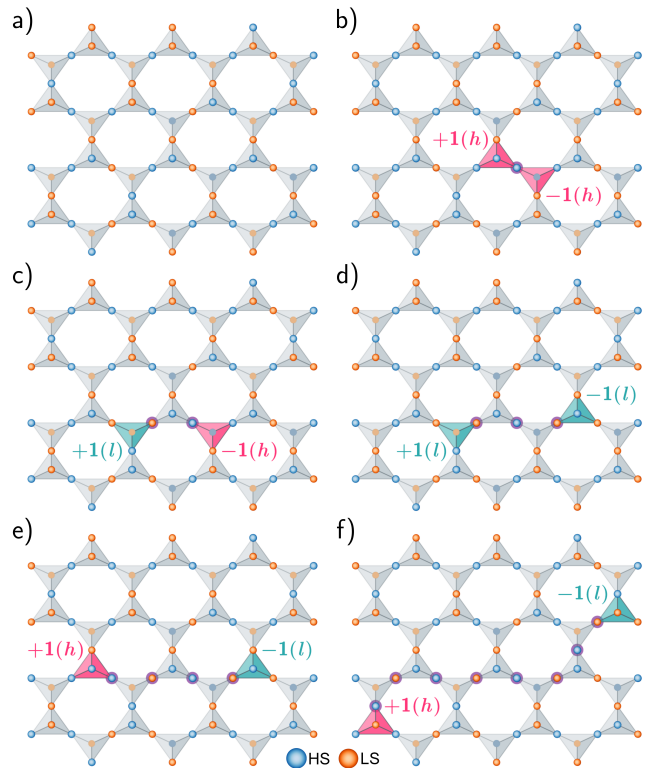


FIG. 5. Sketch of the propagation of defects in the  $H_2L_2$  phase. (a) The  $H_2L_2$  vacuum state, every tetrahedron obeys the 2HS/2LS spin-state ice rule. (b) Changing the spin-state of a LS metal center (highlighted in purple) creates  $h$  defects, on both tetrahedra connected to the metal, but does not change the total topological charge,  $\sum Q = \sum \kappa\delta S$ , where,  $\kappa = \pm 1$  for tetrahedra pointing in the  $\pm z$  direction, and the sum runs over all tetrahedra. (c-f) Additional spin-state changes on tetrahedra hosting defects are low-energy process and cause the defects to propagate. This conserves  $Q$ , but not the numbers of  $h$  or  $l$  defects. Similar processes result in deconfined excitations in both the  $H_1L_3$  and  $H_3L_1$  SSI phases.

of SCO molecules could also allow for the use of pressure and light to manipulate and control the excitations.

Important questions arising from this work include: what are the leading quantum mechanical corrections to the Hamiltonian? and what state do they lead to? Based on analogies to spin ice and the dimer/loop models on the diamond lattice [1, 3] one would expect that significant tunneling between the classical ground states would replace the multiple SSI phases with  $U(1)$  quantum spin-state liquid phases.

This work was funded by the Australian Research Council through grant number DP200100305 and an Australian Government Research Training Program Scholarship.

- 
- \* j.cruddas@uq.edu.au  
 † powell@physics.uq.edu.au
- [1] C. Castellano, R. Moessner, and S. L. Sondhi, *Spin Ice, fractionalization and Topological order*, *Ann. Rev. Condens. Matter Phys.* **3**, 35 (2012).
- [2] C. L. Henley, *Coulomb phases*, *Annu. Rev. Condens. Matter Phys.* **1**, 179–210 (2010).
- [3] L. Savary and L. Balents, *Quantum spin liquids: a review*, *Rep. Prog. Phys.* **80**, 16502, (2017).
- [4] E. Lefrançois, V. Cathelin, E. Lhotel, J. Robert, P. Lejay, C. V. Colin, B. Canals, F. Damay, J. Ollivier, B. Fåk, L. C. Chapon, R. Ballou and V. Simonet, *Fragmentation in spin ice from magnetic charge injection*, *Nat. Comm.* **8**, 209 (2017).
- [5] J. Cruddas, B. J. Powell, *Spin-state Ice in elastically frustrated spin-crossover materials*, *J. Am. Chem. Soc.*, **141**, 19790 (2019).
- [6] P. Gütllich, Y. Garcia and H. A. Goodwin, *Spin crossover phenomena in Fe(II) complexes*, *Chem. Soc. Rev.*, **29**, 419 (2000).
- [7] O. Kahn, J. Kröber and C. Jay, *Towards Spin Crossover Applications*, *Adv. Mater.*, **4**, 718 (2004).
- [8] A. Köbke, F. Gutzeit, F. Röhrich, A. Schlimm, J. Grunwald, F. Tuczec, M. Studniarek, D. Longo, F. Choueikani, E. Otero, P. Ohresser, S. Rohlf, S. Johannsen, F. Diekmann, K. Rosnagel, A. Weismann, T. Jasper-Toennies, C. Näther, R. Herges, R. Berndt and M. Gruber, *Reversible coordination-induced spin-state switching in complexes on metal surfaces*, *Nat. Nanotechnol.*, **15**, 18 (2020).
- [9] H.-Z. Ye, C. Sun, H. Jiang, *Monte-Carlo simulations of spin-crossover phenomena based on a vibronic Ising-like model with realistic parameters*, *Phys. Chem. Chem. Phys.*, **17**, 6801 (2015).
- [10] M. Paez-Espejo, M. Sy, K. Boukheddaden, *Elastic Frustration Causing Two-Step and Multistep Transitions in Spin-Crossover Solids: Emergence of Complex Antiferroelastic Structures*, *J. Am. Chem. Soc.*, **138**, 3202 (2016).
- [11] C. Mariette, E. Trzop, J.-Y. Mevellec, A. Boucekine, A. Ghoufi, G. Maurin, E. Collet, M. Carmen Muñoz, J. A. Real, and B. Toudic, *Symmetry breakings in a metal organic framework with a confined guest*, *Phys. Rev. B* **101**, 134103 (2020).
- [12] J. Pavlik and R. Boča *Established Static Models of Spin Crossover*, *Eur. J. Inorg. Chem.* **2013**, 697-709 (2013).
- [13] M. Nishino, K. Boukheddaden, Y. Konishi, and S. Miyashita, *Simple Two-Dimensional Model for the Elastic Origin of Cooperativity among Spin States of Spin-Crossover Complexes*. *Phys. Rev. Lett.* **98**, 247203 (2007).
- [14] M. Nishino and S. Miyashita, *Termination of the Berezinskii-Kosterlitz-Thouless phase with a new critical universality in spin-crossover systems*, *Phys. Rev. B* **92**, 184404 (2015).
- [15] M. Nishino, C. Enachescu, and S. Miyashita, *Multistep spin-crossover transitions induced by the interplay between short- and long-range interactions with frustration on a triangular lattice*, *Phys. Rev. B* **100**, 134414 (2019).
- [16] S. Miyashita, Y. Konishi, M. Nishino, H. Tokoro, and P. A. Rikvold, *Realization of the mean-field universal-ity class in spin-crossover materials*, *Phys. Rev. B* **77**, 014105 (2008).
- [17] T. Nakada, T. Mori, S. Miyashita, M. Nishino, S. Todo, W. Nicolazzi, and P. A. Rikvold, *Critical temperature and correlation length of an elastic interaction model for spin-crossover materials*, *Phys. Rev. B* **2012**, *85*, 054408.
- [18] M. Nishino, and S. Miyashita, *Effect of the short-range interaction on critical phenomena in elastic interaction systems*, *Phys. Rev. B* **88**, 014108 (2013).
- [19] H. Watanabe, K. Tanaka, N. Bréfuel, H. Cailleau, J.-F. Létard, S. Ravy, P. Fertey, M. Nishino, S. Miyashita, and E. Collet, *Ordering phenomena of high-spin/low-spin states in stepwise spin-crossover materials described by the ANNNI model*, *Phys. Rev. B* **2016**, *93*, 014419.
- [20] C. Enachescu, L. Stoleriu, M. Nishino, S. Miyashita, A. Stancu, M. Lorenc, R. Bertoni, H. Cailleau, and E. Collet, *Theoretical approach for elastically driven cooperative switching of spin-crossover compounds impacted by an ultrashort laser pulse*, *Phys. Rev. B* **95**, 224107 (2017).
- [21] Y. Konishi, H. Tokoro, M. Nishino, and S. Miyashita, *Monte Carlo simulation of pressure-induced phase transitions in spin-crossover materials*, *Phys. Rev. Lett.* **100**, 067206 (2008).
- [22] L. Stoleriu, P. Chakraborty, A. Hauser, A. Stancu, and C. Enachescu, *Thermal hysteresis in spin-crossover compounds studied within the mechanoelastic model and its potential application to nanoparticles*, *Phys. Rev. B* **84**, 134102 (2011).
- [23] J. Cruddas, B. J. Powell, *Structure-property relationships and the mechanisms of multistep transitions in spin crossover materials and frameworks*, arXiv:2006.03255.
- [24] A. J. McConnell, *Spin-state switching in Fe(II) helicates and cages*, *Supramol. Chem.*, **30**, 858 (2018).
- [25] W. Nicolazzi, A. Bousseksou, *Thermodynamical aspects of the spin crossover phenomenon*, *C. R. Chimie*, **21**, 1060 (2018).
- [26] J. Wajnflasz and R. Pick, *Transitions «Low Spin»-«high Spin» dans les complexes de Fe<sup>2+</sup>*, *J. Phys. Colloques*, **32**, C1-91-C1-92 (1971).
- [27] E. Collet, H. Watanabe, N. Bréfuel, L. Palatinus, L. Roudaut, L. Toupet, K. Tanaka, J.-P. Tuchagues, P. Fertey, S. Ravy, B. Toudic, and H. Cailleau, *Aperiodic Spin State Ordering of Bistable Molecules and Its Photoinduced Erasing*, *Phys. Rev. Lett.* **109**, 257206 (2012).
- [28] J. E. Clements, J. R. Price, S. M. Neville, and C. J. Kepert, *Hysteretic Four-Step Spin Crossover within a Three-Dimensional Porous Hofmann-like Material*, *Angew. Chem. Int. Ed.* **55**, 15105–15109 (2016).
- [29] M. J. Murphy, K. A. Zenere, F. Ragon, P. D. Southon, C. J. Kepert, and S. M. Neville, *Guest Programmable Multistep Spin Crossover in a Porous 2-D Hofmann-Type Material*, *J. Am. Chem. Soc.* **139**, 1330-1335 (2017).
- [30] M. Griffin, S. Shakespeare, H. J. Shepherd, C. J. Harding, J.-F. Létard, C. Desplanches, A. E. Goeta, J. A. K. Howard, A. K. Powell, V. Mereacre, Y. Garcia, A. D. Naik, H. Müller-Bunz, and G. G. Morgan, *A Symmetry-Breaking Spin-State Transition in Iron(III)*, *Angew. Chem. Int. Ed.* **50**, 896–900 (2011).
- [31] Y. Sekine, M. Nihei, and H. Oshio, *Dimensionally Controlled Assembly of an External Stimuli-Responsive [Co<sub>2</sub>Fe<sub>2</sub>] Complex into Supramolecular Hydrogen-Bonded Networks*, *Chem. Eur. J.* **23**, 5193-5197 (2017).
- [32] N. Ortega-Villar, A.L. Thompson, M.C. Muñoz, V.M. Ugalde-Saldívar, A.E. Goeta, R. Moreno-Esparza and

- J.A. Real, *Solid- and Solution-State Studies of the Novel  $\mu$ -Dicyanamide-Bridged Dinuclear Spin-Crossover System  $[\text{Fe}(\text{bztpen})]_2[\mu\text{-N}(\text{CN})_2](\text{PF}_6)_3 \cdot n\text{H}_2\text{O}$* , Chem. Eur. J. **11**, 5721-5734 (2005).
- [33] G.S. Matouzenko, D. Luneau, G. Molnár, N. Ould-Moussa, S. Zein, S.A. Borshch, A. Bousseksou and F. Averseng, *A Two-Step Spin Transition and Order-Disorder Phenomena in the Mononuclear Compound  $[\text{Fe}(\text{Hpy-DAPP})](\text{BF}_4)_2$* , Eur. J. Inorg. Chem. **13**, 2671-2682 (2006).
- [34] See Supplementary Information for detailed expressions for the diffuse and Bragg scattering, plots of the heat capacity;  $n_{HS}$  from parallel tempering, heat and cooling; and snapshots of the ice states.
- [35] E. Milin, V. Patinec, S. Triki, E.-E. Bendeif, S. Pillet, M. Marchivie, G. Chastanet, and K. Boukheddaden, *Inorg. Chem.*, **2016**, 55, 11652.
- [36] V. B. Jakobsen, E. Trzop, L. C. Gavin E. Dobbelaar, S. Chikara, X. Ding, K. Esien, H. Müller-Bunz, S. Felton, V. S. Zapf, E. Collet, M. A. Carpenter, and G. G. Morgan, *Stress-Induced Domain Wall Motion in a Ferroelastic  $\text{Mn}^{3+}$  Spin Crossover Complex* Angew. Chem. Int. Ed. doi:10.1002/anie.202003041 (2020).

**Supplementary Information for “Multiple Coulomb phases with  
temperature tunable ice rules in pyrochlore spin crossover materials”**  
Jace Cruddas and B. J. Powell

$$S_d(B^z) = S_L(S_L + 1) - m_-^2 + [S_H(S_H + 1) - S_L(S_L + 1) - m_+^2 + m_-^2] n_{HS} \quad (S1)$$

$$S_B(B^z) = \left( \frac{m_+^2 + m_-^2 + 2m_+m_-}{4} \right) + \left( \frac{m_+^2 - m_-^2}{2} \right) (2n_{HS} - 1). \quad (S2)$$

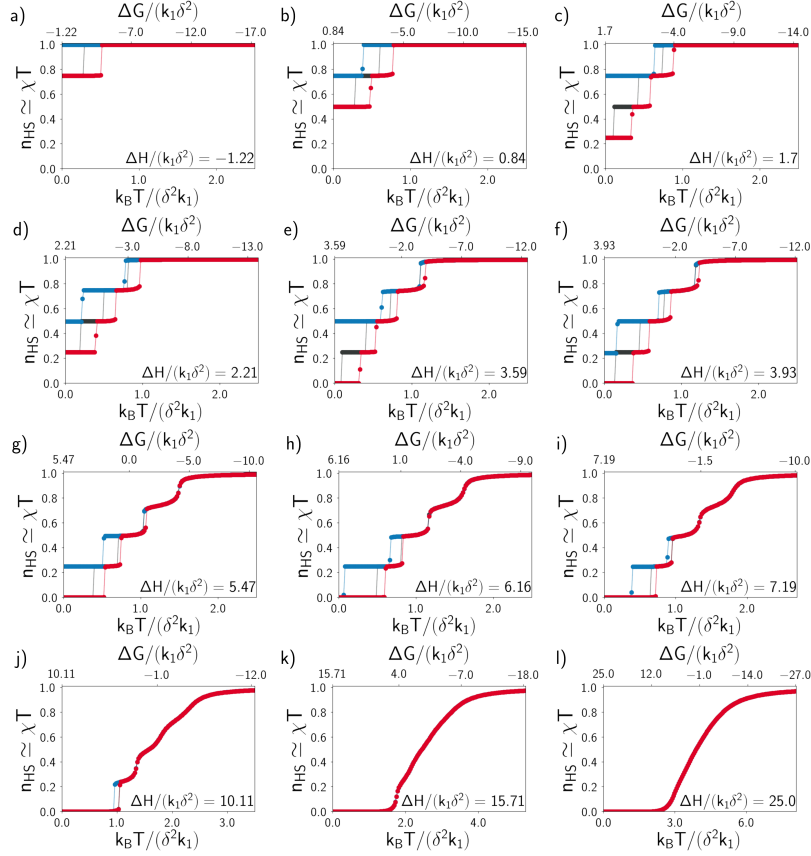


FIG. S1. (As Fig. 4 but with results for parallel tempering added.) The fraction of high spins,  $n_{HS}$ , for selected values of  $\Delta H/(k_1 \delta^2)$  with  $k_1 > 0$  and  $k_2/k_1 = 4k_3/3k_1 = -0.1$ . The red, blue and black lines represent heating, cooling and parallel tempering results, respectively.

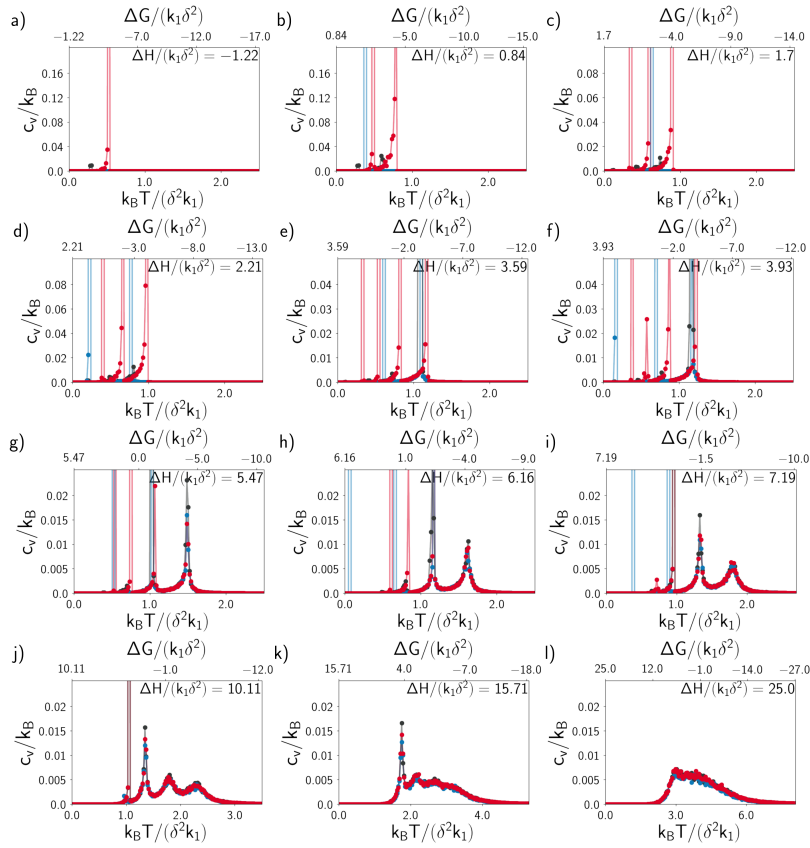


FIG. S2. The heat capacity per site  $c_V$  for the same values of  $\Delta H/(k_1\delta^2)$  as Fig. 4 with fixed values of  $k_1 > 0$  and  $k_2 = 4k_3/3 = -0.1k_1$ . The black, blue and red lines have the same meaning as Fig. 4. Similarly, for increasing values of  $\Delta H/(k_1\delta^2)$  we observe (in the equilibrium values) (a) a first order-transition, (b) two first order transitions, (c-d) three first order transitions, (e-f) four first order transitions, (f-g) three first order transitions and a crossover, (i) two first order transitions and two crossovers, (j) one first order transition and three crossovers, (k) two crossovers and (l) a crossover. Heating and cooling the system would result in (a) no transitions, (b-c) one first order transition, (d-e) two first order transitions, (f) a three-step transition and (g) two-first order transitions.

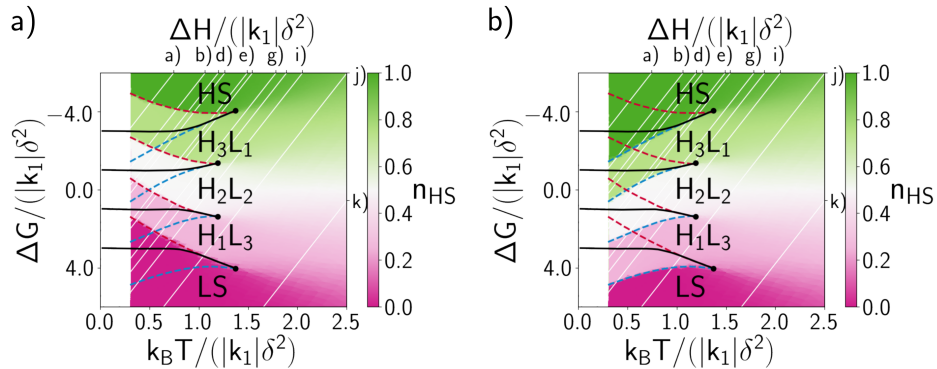


FIG. S3. The HS fraction,  $n_{HS}$ , calculated on (a) cooling and (b) heating for the third nearest neighbor elastic model on the pyrochlore lattice with fixed values of  $k_1 > 0$  and  $k_2 = (4/3)k_3 = -0.1k_1$ . Lines and dots have the same meanings as in Fig. 4a.



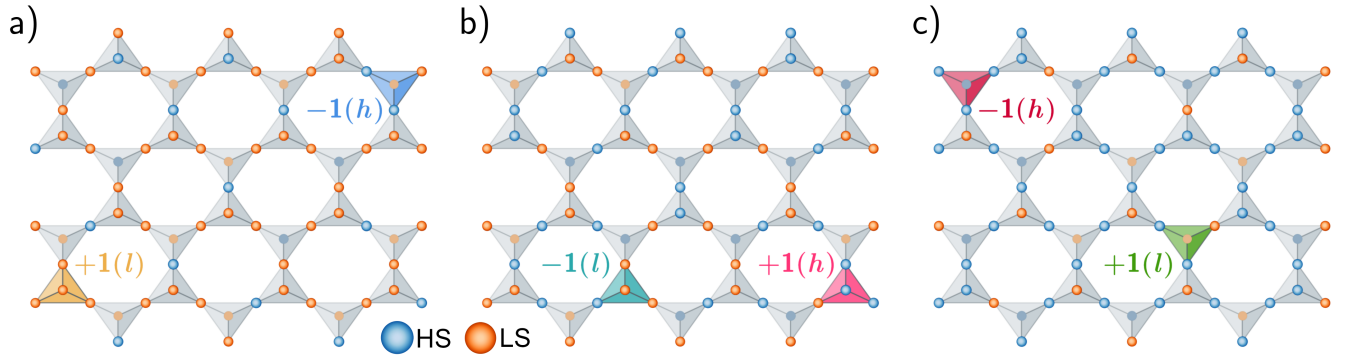


FIG. S4. Truncated snapshots of (a)  $H_1L_3$ , (b)  $H_2L_2$  and (c)  $H_3L_1$  for  $k_1 > 0$  and  $k_2 = 4k_3/2 = -0.1k_1$ . Almost all tetrahedra obey the spin-state ice rules, Fig. 1. There are two expectations to the rule; one tetrahedron containing an excess of HS ( $h$ ) and one containing an excess of LS ( $l$ ). The snapshots are taken for (a)  $\Delta H = 10.11k_1\delta^2$  and  $k_B T = 1.12k_1\delta^2$ , (b)  $\Delta H = 5.47k_1\delta^2$  and  $k_B T = 0.76k_1\delta^2$  and (c)  $\Delta H = 5.47k_1\delta^2$  and  $k_B T = 1.11k_1\delta^2$ .